

# Voltage stability of a photovoltaic DC microgrid using fuzzy logic controller

Kalangiri Manohar, Kottala Padma

Department of Electrical Engineering, Andhra University College of Engineering, Visakhapatnam, India

## Article Info

### Article history:

Received May 21, 2023

Revised Aug 6, 2023

Accepted Aug 31, 2023

### Keywords:

DC-DC converters

Electric vehicles

Fuzzy logic controller

Microgrid

PV array

## ABSTRACT

This article employs a fuzzy logic controller (FLC) to investigate voltage stability in a PV-based DC microgrid. Several photovoltaic (PV) modules, a DC-DC converter, and loads make up the microgrid. Due to the widespread use of intermittent PV power, voltage stability is a crucial problem for DC microgrids and is difficult to accomplish. This study proposes an FLC-based voltage control technique that leverages input factors including PV output power, DC-DC converter duty cycle, and load current to identify the best course of action for preserving the system's voltage stability. The FLC's performance is assessed by simulation, and it is meant to be resilient to parameter fluctuations and uncertainties. The simulation results demonstrate that the suggested FLC-based control strategy successfully maintains the microgrid's voltage stability under a variety of operational circumstances, including changing solar irradiance and load variations. Moreover, the FLC performs better than other control methods.

This is an open access article under the [CC BY-SA](#) license.



## Corresponding Author:

Kalangiri Manohar

Department of Electrical Engineering, Andhra University College of Engineering

Visakhapatnam, Andhra Pradesh, India

Email: kalangirimanohar23@gmail.com

## 1. INTRODUCTION

The solar DC microgrid system's bus voltage serves as a reference point for assessing the system's safety and stability [1]–[3]. Nonetheless, because of the unexpected and fluctuating nature of solar power output, along with dynamic demand variations, the practical functioning of the photovoltaic (PV) DC microgrid introduces unanticipated power disruptions, resulting in large swings in the bus voltage. As a result, assuring power quality and sustaining the DC bus voltage stability emerge as critical issues that require rapid attention. Compensation is now provided by an energy storage device (ESD) combined with the DC bus using a bidirectional converter (BDC) [4]. The micro power source may deliver energy when the load consumes power based on the load bus capacity, improving system resilience [5].

Currently, energy storage unit converters use the voltage and current dual closed-loop control (DCLC) approach. Furthermore, within the framework of classical control theory, the traditional method uses two closed-loop voltage and current controls, with the inner control loop being energy-storing inductance and the outer control loop being the bus voltage, with the proportional integral (PI) controller compensating [6]. This typical control strategy, however, falls short of adequately managing the significant variations and repercussions thereby enhancing the overall dynamic responsiveness of the system, connected with the DC bus voltage.

Many researchers solve the aforementioned issue by combining the feedforward control approach by utilizing the standard DCLC [7]. Depending on the feedforward variables evaluated, these systems can be classified as current feedforward or power feedforward. Takei *et al.* [8], for example, offered three ways for

investigating feedforward load current regulation with the goal of correcting the boost converter's unstable zero point. These techniques outperformed feedback control in terms of reducing voltage changes and improving overall system stability, especially when the output filter capacitance was lowered. In addition, Hou *et al.* [9] expanded on direct power control by implementing a load current feedforward system, in which the load current was passed forward to the control loop. The experimental and simulation findings demonstrated that this load current feedforward strategy considerably enhanced the dynamic responsiveness of DC converters and efficiently maintained a steady output voltage even when the load changed abruptly. Besides, Lu *et al.* [10], The present inner loop control, which depends on the buck converter, features a system for ripple correction carried out using load current feedforward to evolution of the accurateness of the system's output power and accelerate the reaction time of the inner loop dynamics. The aforementioned current feedforward control technique improves the system's dynamic response performance in part. The output current will still respond to load perturbations more slowly than other system responses due to the inherent delays in both the voltage and current loops.

Power feedforward control, like current feedforward control, injects disturbance power into the control loop to reduce bus voltage variations [11]. Recognizing the issue of DC bus fluctuation due to an imbalance between power production from nonconventional sources and load consumption in a DC microgrid, Zhi-Lin *et al.* [12] suggested an approach to power feedforward compensation control based on DCLC that is standard. Through the feedforward channel, the controller receives power disturbances, thereby minimizing bus voltage oscillations and enhancing overall system stability. Song *et al.* [13] created a method called virtual direct power control, which is an extension of direct power feedforward control. This approach aimed to increase the resistance of the bidirectional converter to load disturbances by eliminating the need to consider parameters such as the energy storage inductance of the converter and the fluctuating transformer ratio, hence improving overall system compatibility. The power feedforward method significantly increases the system's response time to power disturbances, allowing it to control bus voltage fluctuations better. Nonetheless, power feedforward control, like current feedforward control, goes through the current inner loop, resulting in a delay in output current response to load disturbances. Meanwhile, it is critical to recognize that applying feedforward control necessitates the collecting of real-time data on system parameters, which raises the cost of the system and diminishes its dependability. This is detrimental to the growth of microgrids and the general acceptance of plug-and-play functionality [14]. Because of the models' relatively simple structure, expensive mathematical computations are avoided in order to achieve the system's real-time necessities.

Given the photovoltaic DC microgrid's obvious nonlinearity and time variability, this work proposes a fuzzy controller as a substitute for the standard dual closed-loop control. In circumstances with high change in bus voltage, to achieve better transient performance, the fuzzy controller is used. In order to provide optimal steady-state performance, the PI controller is employed when the bus voltage variance is moderate. The studies show that both fuzzy control and PI control provide advantages such as quick reaction, little overshoot, high resilience, and robust anti-interference capabilities across a wide range of operational situations.

## 2. ABOUT MICROGRID SYSTEM

Figure 1 depicts the investigated 48-V DC microgrid ring along with the microgrid running in island mode, power balancing is only accomplished through management of distributed energy supplies and compensating devices. The microgrid is constructed from three DC buses that are linked to their respective subsystems and are governed by their respective regional controllers (LCs). Loads are connected to each bus and dispersed across the system.

### 2.1. Solar photovoltaic system

The SPV system, which includes a battery storage system, is coupled to bus and is affected by changes in irradiance and temperature. The boost converter uses maximum power point tracking (MPPT) and an incremental conductance (InC) technique, as well as added integral regulator robustness, to extract the most power from the SPV array. More complex MPPT techniques can be used instead if necessary. When the system's InC and system conductance are equal, which corresponds to the PV power's lowest rate of change, the search for the applied PV voltage in this InC approach comes to an end. The following is how this is expressed mathematically [15].

$$\frac{dP_{PV}}{dV_{PV}} \approx 0 \quad (1)$$

Substituting for  $P_{PV} = V_{PV}I_{PV}$  in (1), we get:

$$\frac{d((V_{PV})(I_{PV}))}{dV_{PV}} \approx 0 \tag{2}$$

where,  $V_{PV}I_{PV}$  are the PV panel's output current and voltage across it, respectively.

$$I_{PV} \frac{dV_{PV}}{dV_{PV}} + V_{PV} \frac{dI_{PV}}{dV_{PV}} \approx 0 \tag{3}$$

$$I_{PV} + V_{PV} \frac{dI_{PV}}{dV_{PV}} \approx 0 \tag{4}$$

$$\frac{dI_{PV}}{dV_{PV}} = -\frac{I_{PV}}{V_{PV}} \tag{5}$$

Utilizing a DC-DC converter with the InC algorithm directs the PV array's operating point towards satisfying in (5).

Figure 1 shows that the complete system related to solar PV based DC micro grid. By using constant voltage mode in its converter, the battery controls the bus voltage, enabling the SPV's converter to run in constant current mode (CCM) and provide the microgrid with the most efficient power. It ensures that the SPV system operates continuously under maximum power point tracking (MPPT) by storing any extra energy generated in the battery.

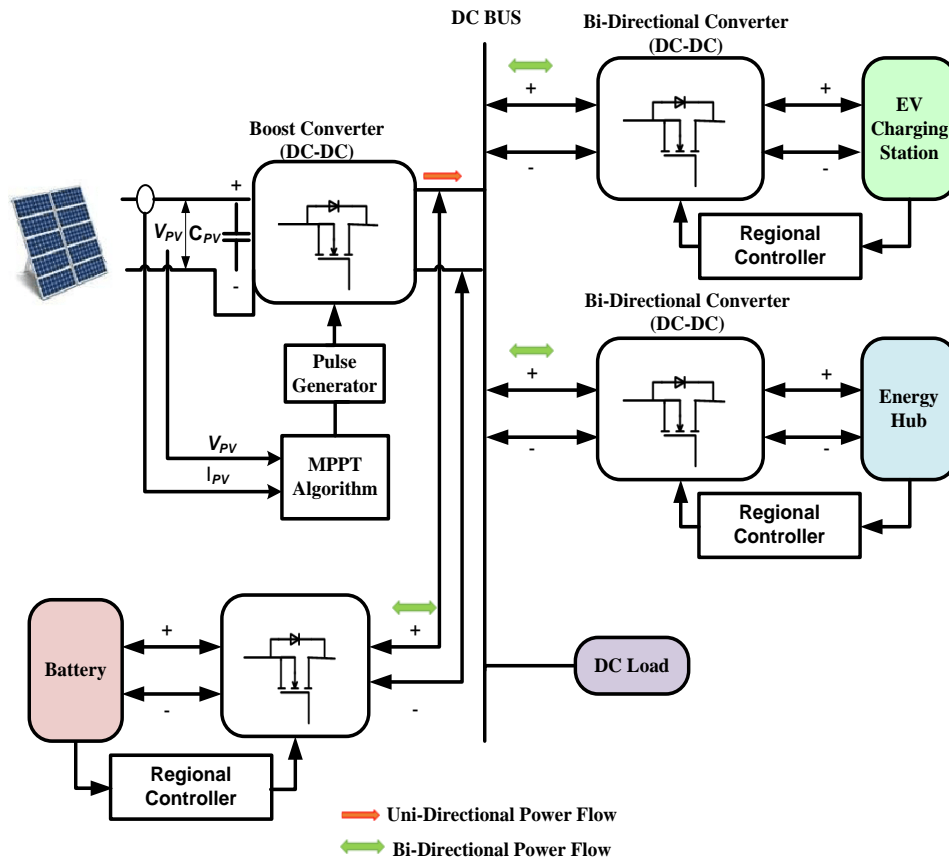


Figure 1. Solar PV based DC microgrid system

Figure 2 shows the detailed circuit representation of the subsystem. The SPV system includes a unidirectional converter that uses MPPT, whereas the bus voltage is controlled by a PI controller in the battery's bidirectional converter. When there is surplus power, the microgrid charges the battery storage, and the battery's charging current is carefully controlled to keep the bus voltage within a reasonable range. The battery's PI control technique makes use of a single integrated regulator.

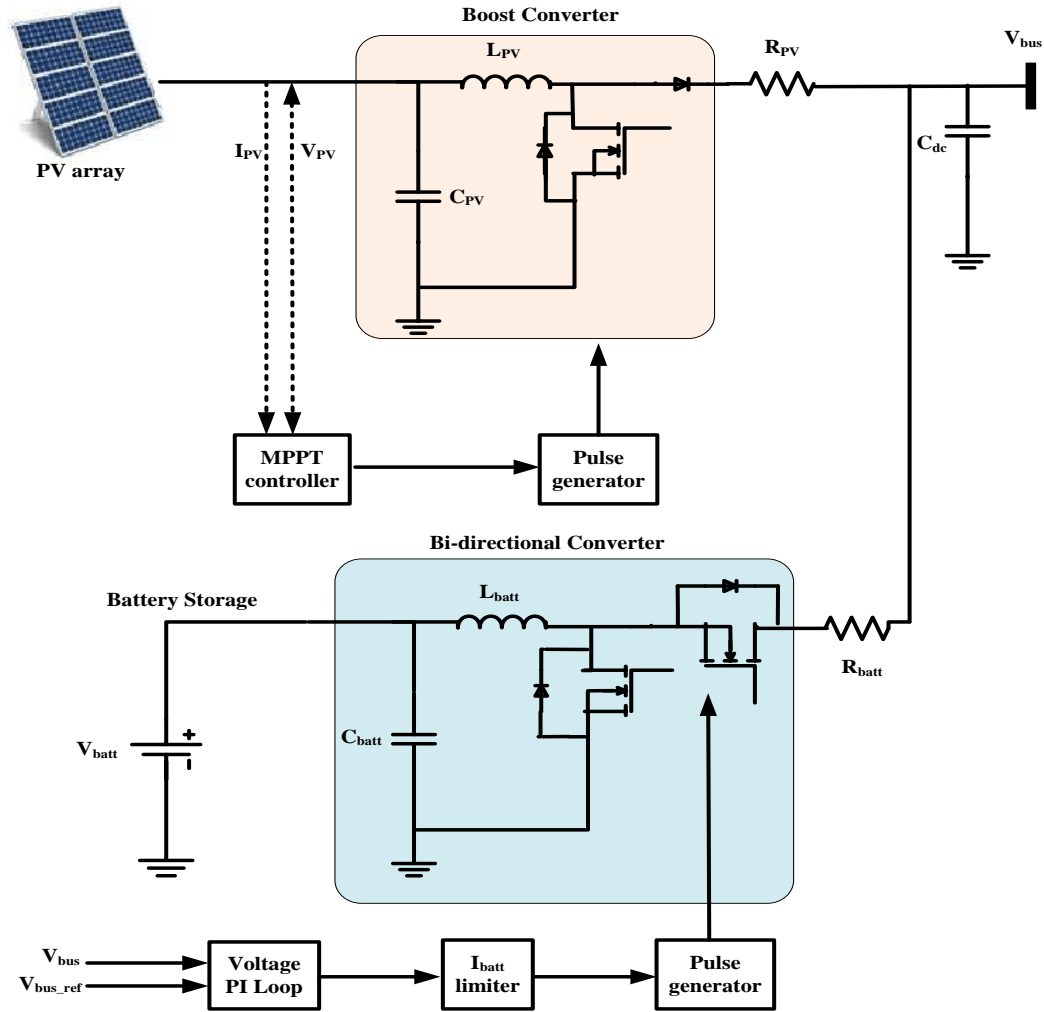


Figure 2. Implemented SPV-battery system

**2.2. Bidirectional DC-DC converter**

DC-DC power converters are critical components of DC microgrid systems because they convert electricity from different voltage levels to the required values. However, common DC converters can only transmit power in one way, which limits the flow of power in two directions to parallel converters. To solve this, the suggested method employs bidirectional converters, as seen in Figure 3, to make storage devices, including batteries and supercapacitors, easier to charge and discharge. Parasitic resistances for inductors and capacitors are used to create the dynamic model of the converter, and they are represented by Inductance, capacitance, input voltage, the load, inductor current, capacitor current, and voltage across the capacitor are represented by the circuit components RL and RC, which are designated as Vi, Vc, IL, IC, L, C, and R. Here S1 and S2 are the symbols of the switches used in the circuit configuration.

The system state space model is represented as (6) and (7).

$$x^{\prime} = Ax + Bu \tag{6}$$

$$y = Cx + Du \tag{7}$$

By averaging the individual SSMs for i) S1 is ON and S2 is OFF for d1 duty cycle (8), the SSM for the converter can be obtained and ii) for a duty cycle of d2 = 1-d1, S1 is OFF, while S2 is ON (9). The selected state variables are:

$$x^{\prime}_{d1} = \begin{pmatrix} \frac{-R_L}{L} & 0 \\ 0 & \frac{-1}{C(R+R_C)} \end{pmatrix} x + \begin{pmatrix} \frac{1}{L} \\ 0 \end{pmatrix} u \tag{8}$$

$$x'_{d2} = \begin{pmatrix} \frac{1}{L} \left( R_L + \frac{RR_C}{R+R_C} \right) & \frac{-1}{L} \left( 1 + \frac{R_C}{R+R_C} \right) \\ \frac{R}{C(R+R_C)} & \frac{-1}{C(R+R_C)} \end{pmatrix} x + \begin{pmatrix} \frac{1}{L} \\ 0 \end{pmatrix} u \tag{9}$$

with the use of (10) and (11) and the averaged SSM model, (12) may be created:

$$A = d_1 A_1 + d_2 A_2 \tag{10}$$

$$B = d_1 B_1 + d_2 B_2 \tag{11}$$

$$\begin{pmatrix} \frac{1}{L} \left( R_L(1 - 2d) + \frac{RR_C}{R+R_C} \cdot d' \right) & \frac{-1}{L} \left( 1 + \frac{R_C}{R+R_C} \right) \cdot d' \\ \frac{R(1-d)}{C(R+R_C)} & \frac{-1}{C(R+R_C)} \end{pmatrix} x + \begin{pmatrix} \frac{1}{L} \\ 0 \end{pmatrix} u \tag{12}$$

Similar methods can be used to derive the C, D, resulting in (13).

$$y = \begin{pmatrix} 1 & 0 \\ 0 & 1 \end{pmatrix} x + \begin{pmatrix} \frac{1}{L} \\ 0 \end{pmatrix} u \tag{13}$$

The converter is depicted within a complete switching cycle of duration  $T_s$  in this ultimate averaged SSM.

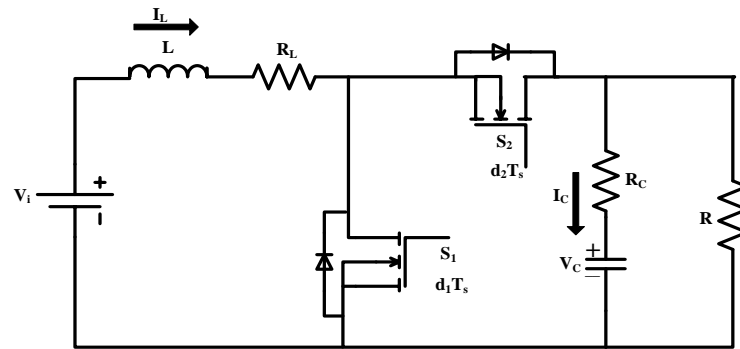


Figure 3. Implemented bidirectional DC-DC converter

**2.3. Energy hub system**

These systems have two main functions: they work as a power source when the microgrid's production cannot keep up with the demand from the load, and they act as a power storage when the production is available. Traditional compensation methods involve the use of battery storage devices that can discharge and charge based on the microgrid's power level. However, due to the slow dynamic response of batteries, rapid load power increases or decreases in renewable power require additional compensation in DC microgrid power balancing. Super capacitors (SCap) offer rapid response times and high instantaneous output power. So, before the battery achieves steady operation, SCap utilizes to compensate for sudden power requirements. By shielding the battery from undue stress during big power transients, this improves performance and increases battery life.

Energy Hubs are included in the suggested design for the following reasons, during times of heavy demand in the microgrid, the SCap absorbs substantial transients, and the battery helps sustain the bus voltage. Without these mechanisms, the microgrid's power regulation and balancing would be dependent on controlling the outputs of generators like the SPV unit. However, generation units must produce the most electricity feasible during periods of high demand. We may relieve the generation units of the control burden by utilizing the Energy Hub. This enhances the microgrid's ability to regulate and balance power. As shown in Figure 4, the energy hub is made up of a SCap that is linked to the same DC bus utilizing BDCs. The supercapacitor control uses a cascaded PI method to make sure that the steady-state value of  $i_{sc}$  is decreased to zero while the battery control controls the bus voltage.

**2.4. About charging station of the electric vehicle (EV)**

The integration of vehicle-to-grid (V2G) technology in microgrids has facilitated the transfer of compensation load to electric vehicles (EVs) when they are connected to charging stations. The advantages

and difficulties associated with implementing this technology have been explored in [16]. The complete architecture of the micro grid system with multiple EVs is depicted in Figure 5.

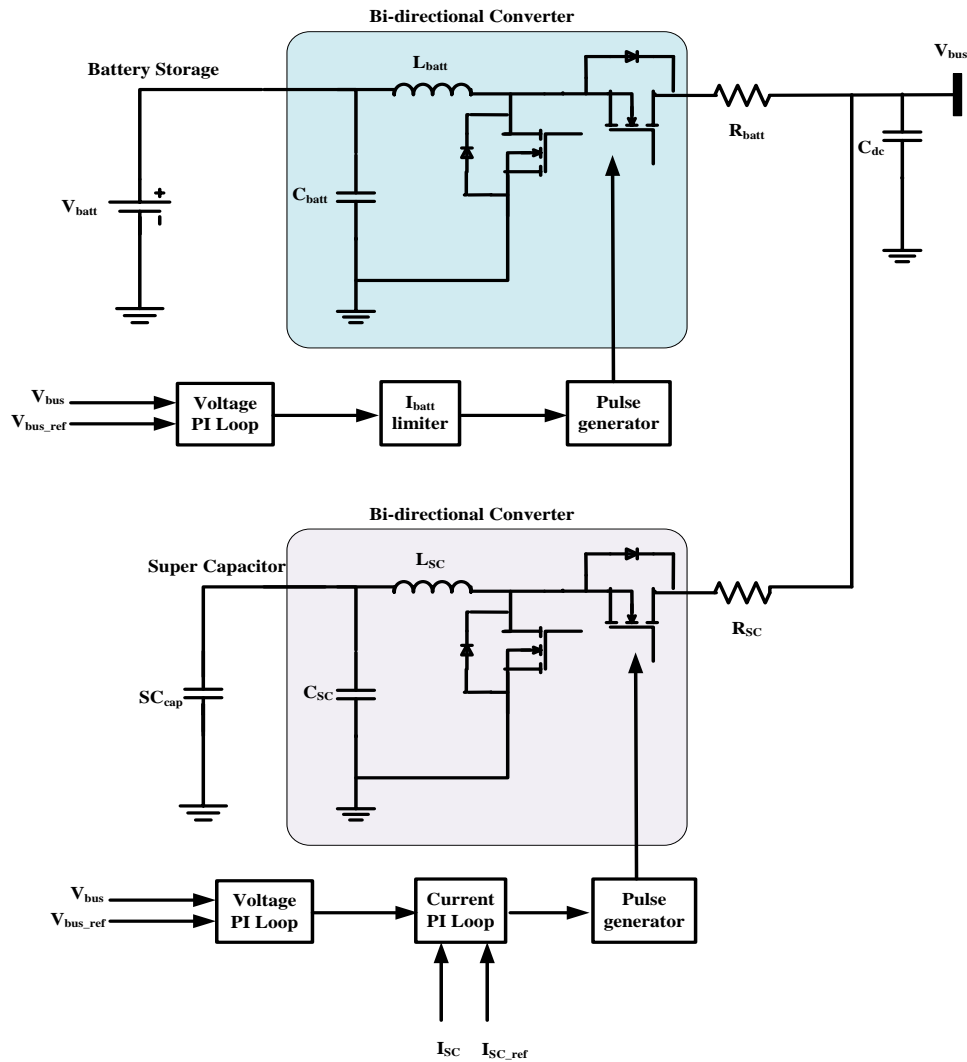


Figure 4. Implemented energy hub system

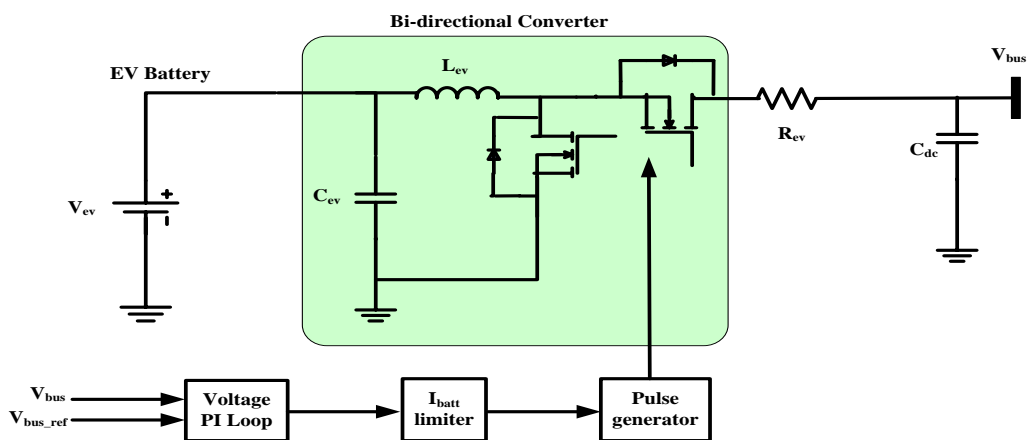


Figure 5. Implemented EV charging station system

### 3. PROPOSED CONTROL TECHNIQUE

A distributed control mechanism is used in this work, to provide power management in a DC microgrid. This does not necessitate the use of a communication network. Interconnected DC/DC converters manage the power flow from each individual source.

#### 3.1. Conventional droop control

The advancements in power electronics have rendered the decentralized approach to microgrids more cost-effective and easily available. However, to achieve this, the regional controller must rely significantly on the regional variable, thereby making the regional variable more crucial for the control system. Droop control is a parallel technique that can be controlled without feedback and does not require additional wiring for data transfer. This makes droop control is the generally utilized technique as it ensures well-balanced voltage and current management [17]. The traditional strategy for droop control is described as (14).

$$V_{dck} = V_{dc} - I_{dck}R_{dk} \tag{14}$$

The traditional systems performance significantly influenced by the impedance of the transmission line. Both linear and nonlinear approaches can be employed in droop control. Additionally, line resistance possesses another drawback by causing uneven minimal voltage and load distribution, thereby reducing the equivalence in power sharing. When the nominal voltages have zero error, all converters connected in parallel handle an equivalent load current. Even a slight deviation in the nominal voltage results in a circulating current will follows the error [18].

#### 3.2. PI controller

The PI controller belongs to the category of proportional integral derivative (PID) controllers, and it generates the necessary duty cycle by considering the output error. The PI controller exhibits greater resistance to noise and disturbances compared to the PID controller. As a result, there are no oscillations in the duty cycle that the PI controller generates. In terms of offset and steady-state error, the PI controller outperforms the PID controller [19]–[22]. With all of these considerations in mind, this study chooses to use a PI controller rather than a PID controller. The equation shown below presents the mathematical analysis of the PI controller.

$$U(t) = K_i \int_0^t e(t)dt + K_p e(t) \tag{15}$$

The error signal  $e(t)$  for the PI controller is given as (16).

$$e(t) = V_{bus} - V_{bus\_ref} \tag{16}$$

Figure 6 shows that, the voltage and current loops are controlled separately by two PI controllers when using the dual-loop control approach. In this method, the converter's output feedback serves as the first controller's direct input. The second controller then uses this output to calculate the required duty cycle. Here Table 1 shows the gain values of the PI controller related to mode of operation pertaining to the type of energy source utilized to drive the electric vehicle.

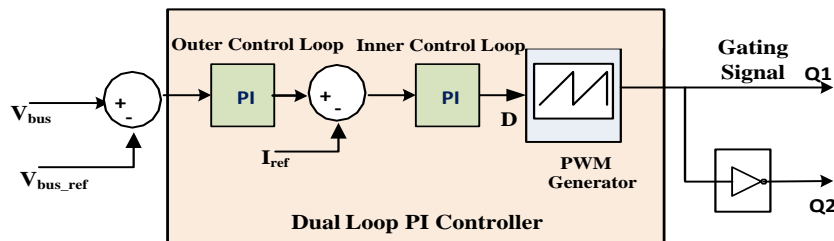


Figure 6. Picture of a dual-loop PI controller in block form

Mode	$K_{pv}$	$K_{iv}$	$K_{pi}$	$K_{ii}$
Battery	0.2	2.45	0.45	2.8
Supercapacitor	0.1	4	0.27	3.2
PV-Battery	0.1	4	10	4

The conventional PI controller tuning lacks the inclusion of a right-half plane zero and does not pay sufficient attention to the converter design. Consequently, this oversight leads to an over-damped output voltage in boost converters [23]–[25]. To overcome this drawback, this paper employs a fuzzy logic controller (FLC) to mitigate the mentioned disadvantage.

### 3.4. Proposed fuzzy logic controller

The FLC control severely relies on the rules established by linguistic variables. Unlike other approaches, fuzzy logic control does not demand complex arithmetic operations. It simply performs straightforward calculations to regulate the model. Despite its reliance on basic mathematics, it effectively operates within a control system. Consequently, this strategy stands as one of the most effective and accessible methods for plant regulation [26]. FLC is based on the concept of fuzzy sets, where each element possesses a membership level indicating its association with a specific set. Fuzzy sets are characterized by less well-defined boundaries compared to classical sets. The fuzzy logic controller (FLC) is commonly employed when precision requirements are minimal, and the plant does not necessitate intricate mathematical analysis. Although it is rooted in fundamental mathematics, the FLC showcases excellent performance within a control system. Hence, it remains one of the most efficient and straightforward approaches to plant control. Fuzzy logic control is founded on the principles of fuzzy set theory, where each element is assigned a membership degree to indicate its belongingness to a particular set. Fuzzy sets share similarities with classical sets but exhibit more flexible boundaries. When moderate accuracy is required, and extensive mathematical analysis is unnecessary, the FLC is the preferred choice. The complete block diagram representation of the FLC is represented in Figure 7.

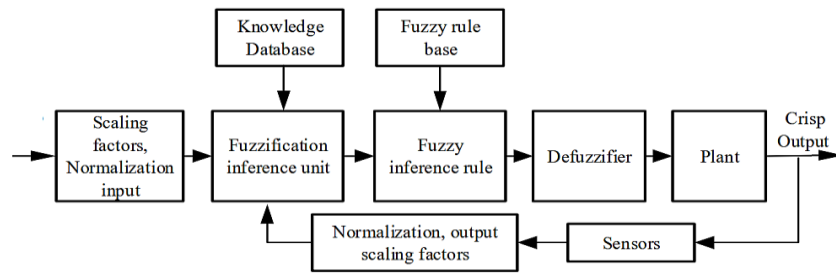


Figure 7. Block diagram of FLC

The FLC devised an optimal switching sequence to facilitate the charging and discharging operations of batteries. Additionally, it receives error indications derived from the comparison between the DC Bus voltage and the reference voltage signal. Based on this information, the fuzzy controller determines the duty cycle to be utilized by the PWM block for signaling the buck/boost converter.

In this study, the FLC with a Mamdani base is used. Two inputs are provided to the FLC: the output voltage error ( $e(t)$ ) and the error change ( $de(t)$ ) from the preceding error. The definitions of  $e(t)$  and  $de(t)$ , and are given in (17) and (18).

$$e(t) = V_{sense}(t) - V_{ref} \quad (17)$$

$$de(t) = e(t) - e(t - 1) \quad (18)$$

Here,  $V_{ref}$  is the necessary output voltage and  $V_{sense}(t)$  is the system's  $t$ th sampled output voltage. It is multiplied by the scaled factors  $k_1$  and  $k_2$  with both input variables before being delivered to the FLC. Following that, the scaled input is assigned the membership functions (MF) in accordance with the fuzzy logic rule. Among of the different MF shapes available, triangular MF is chosen for its simplicity and ease of application. A larger number of fuzzy sets is required for smooth system adjustment; nevertheless, this increases the complexity of MF forms. As a result, there should be a trade-off between the complexity of the MF and the quantity of fuzzy sets used. Seven fuzzy subsets, called negative large (NL), negative medium (NM), negative small (NS), zero (ZE), positive small (PS), positive medium (PM), and positive large (PL), are now allotted to the FLC. L, M, and S stand for big, medium, and small, respectively, while N, P, and Z stand for negative, positive, and zero, respectively. The required duty cycle ( $D$ ) is output by FLC and is delivered to the plant [27]–[29]. Fuzzy control rule sets are assigned based on converter  $7 \times 7$ . Figures 8 and 9 are representing the fuzzy inference system (FIS) editor window and FLC rules viewer in order. Table 2 shows the rules sets for the converter operation based on the error and change in error related to the fuzzy logic controller. Figure 10(a) shows that the error signal value Figure 10(b) represents the derivative of the error signal,

Figure 10(c) shows the derivate for the command signal Figure 10(d) represents the proposed FLC related membership function 3D representation, based on the NB, NM, NS, Z, PS, PM, and PB.

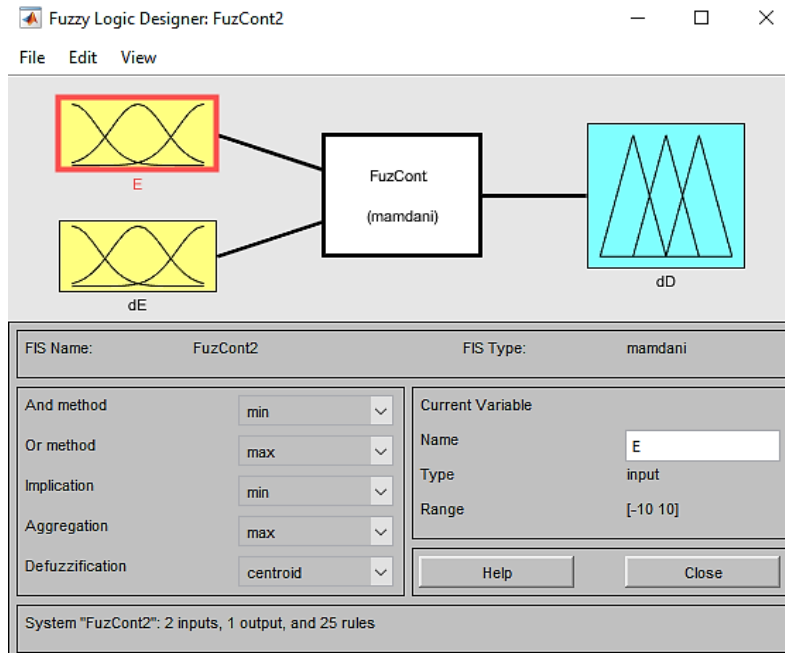


Figure 8. FIS editor window in MATLAB

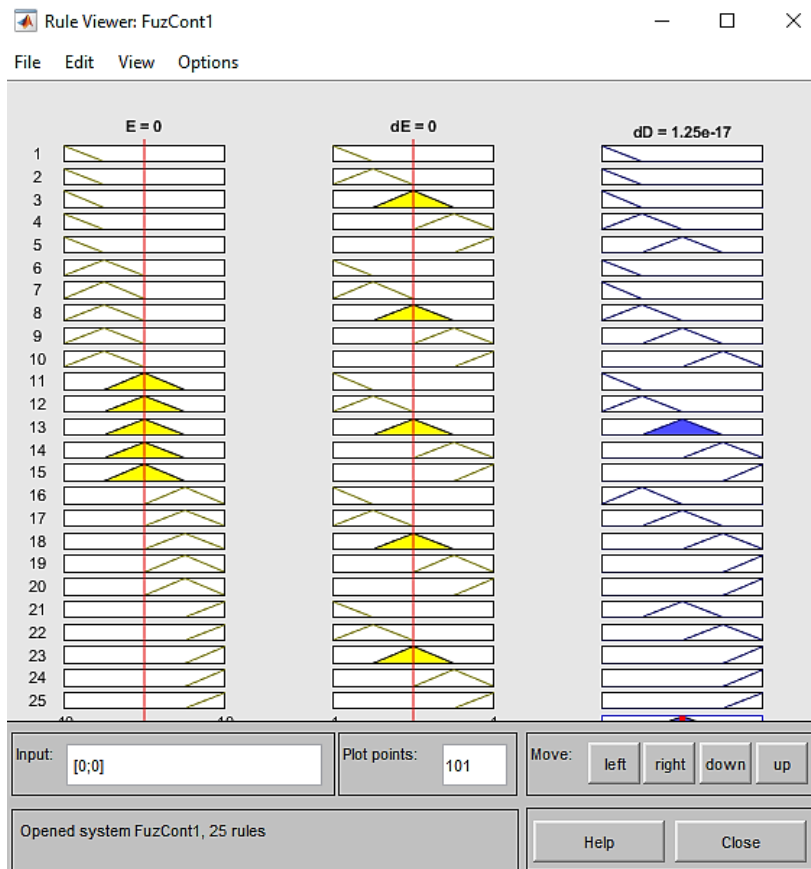


Figure 9. FLC rule viewer

Table 2. Rule sets for converter

$\begin{matrix} de(t) \\ e(t) \end{matrix}$	NL	NM	NS	ZE	PS	PM	PL
NL	NL	NL	NL	NM	NM	NM	ZE
NM	NL	NL	NM	NM	PS	PS	PM
NS	NL	NM	NM	NM	ZE	PS	PS
ZE	NM	NS	ZE	ZE	ZE	ZE	ZE
PS	NM	ZE	PS	PS	PS	PM	PM
PM	NM	ZE	PS	PS	PL	PL	PL
PL	ZE	PM	PS	PL	PL	PL	PL

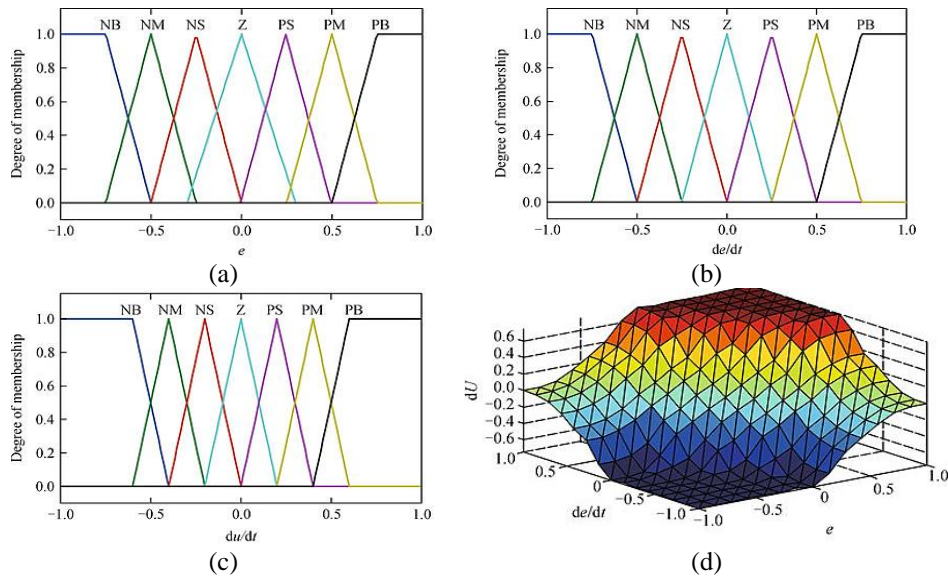


Figure 10. Different structures of FLC (a) error  $e$  (pu), (b) derivative of error  $de/dt$  (pu), (c) derivative of command  $du/dt$  (pu), and (d) surface produced are the membership functions for the proposed FLC

#### 4. MATLAB/SIMULINK RESULTS AND DISCUSSION

The recommended control strategy's reliability and precision in controlling bus voltage regulation and achieving the ideal load distribution under several conditions were evaluated. The following subsections provide an overview of each test's findings. Within this framework, the projected control system underwent an assessment concerning a swift rise followed by a rapid reduction in load, juxtaposed with the droop controller, PI controller, and fuzzy controller. In these instances, the localized controllers employ their distinct control algorithms to rectify fluctuations in bus voltage. The energy hub starts power injection to the microgrid as power generation decreases by initially using the SCap to meets the abrupt power surge till the batteries can reach the new equilibrium value.

##### 4.1. Sudden load changes case

Within this framework, the projected control system underwent an assessment concerning a swift rise followed by a rapid reduction in load, juxtaposed with the droop controller, PI controller, and fuzzy controller. In these instances, the localized controllers employ their distinct control algorithms to rectify fluctuations in bus voltage. The energy hub starts power injection to the microgrid as power generation decreases by initially using the SCap to meets the abrupt power surge till the batteries can reach the new equilibrium value.

The findings in Figure 11 illustrate that the suggested fuzzy control method manages rapid increments/decrements in loading in a robust way, allowing for efficient bus voltage and power regulation. In the droop controller, the highest bus voltage variation was detected. Figure 11(a) represents that the step load changes related to the power in Watts in comparison with three different controllers like droop controller, PI controller, and fuzzy controller. On the other hand, Figure 11(b) shows the voltage changes corresponding to the step load change with three controllers.

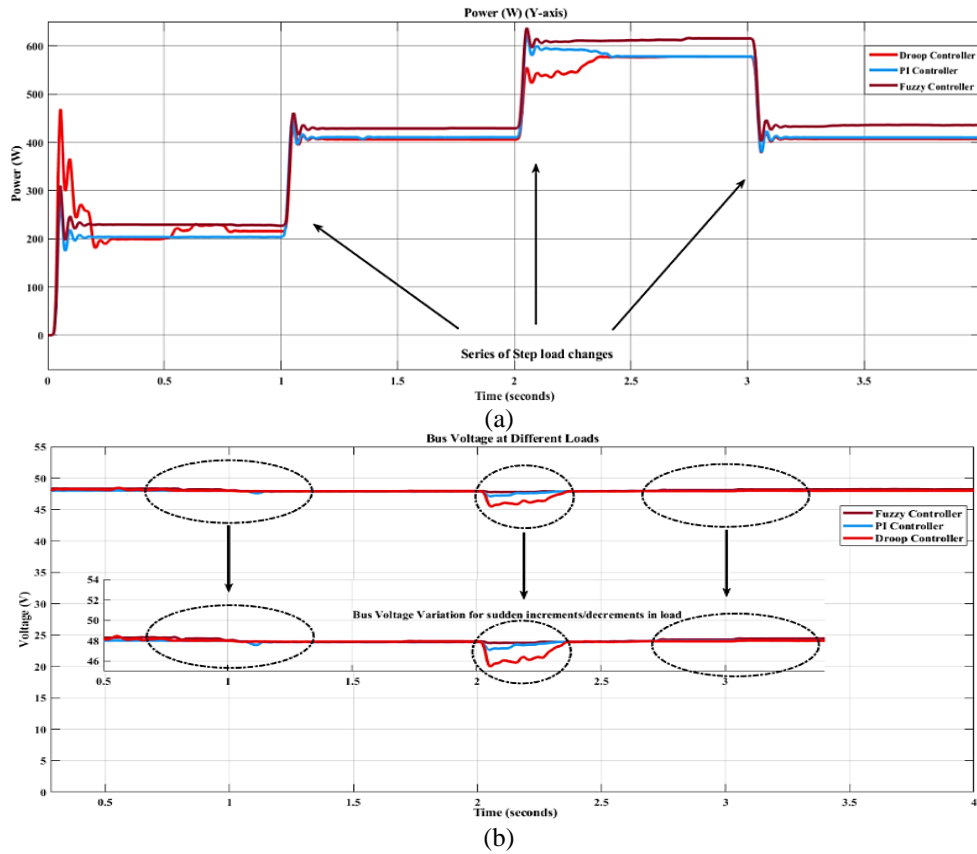


Figure 11. Representation of sudden load change case (a) shows the step-load change in power and (b) shows the step-load change in voltage

#### 4.2. Communication delay

In this particular situation, the suggested control approach underwent assessment to gauge its performance when faced with delays in controller communication. It is crucial to emphasize that this hypothetical scenario is being used to simulate the dispersed mode of the microgrid, where delays are introduced between each regional controller. The strategy was then simulated with each regional controller in the system having a communication latency of 200 ms. The findings are shown in Figure 12. The voltage stabilization time was found to be 0.15 s. The voltage variance is greater with droop control than with PI and fuzzy, but it dies out quickly with the fuzzy controller. Based on this finding, we can conclude that even if there is a communication delay between the regional controllers as a result of the distributed method, the control stabilizes bus voltage.

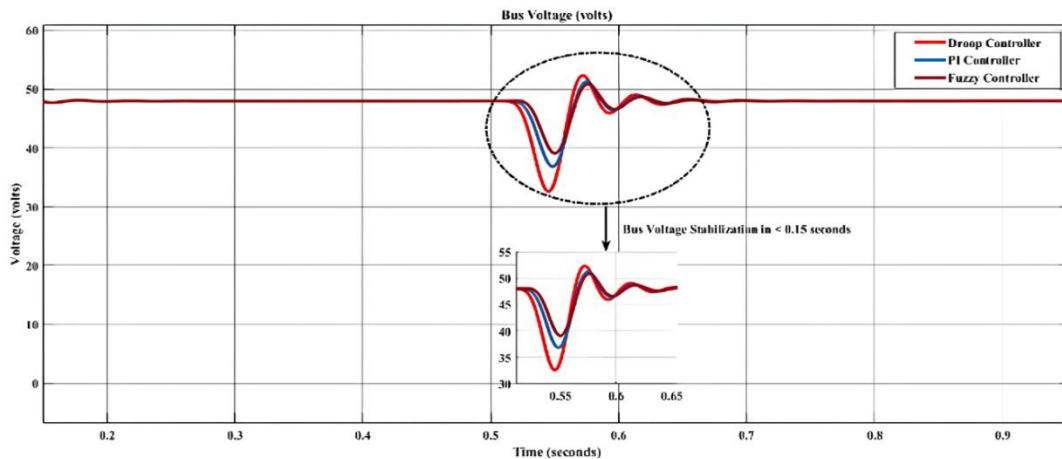


Figure 12. Simulation with communication delay of 200 ms

### 4.3. Batter storage node simulation of the SPV

The results of the simulation indicate a direct correlation between the decrease in solar irradiation and the corresponding decrease in battery charging current, and vice versa. The solar photovoltaic (SPV) system has been given priority over the battery. In the event that the battery reaches full charge, the SPV system works in a de-rated mode. The InC algorithm is employed to maximize power extraction from the SPV system.

Figure 13 represents that the different scenarios were run on the SPV-battery node, including abrupt increases in irradiance (250–1000 W/m<sup>2</sup>), abrupt declines in irradiance (1000–250 W/m<sup>2</sup>), and abrupt changes in load. Temperature variations have also been used to test the system. Figure 13 simulates and shows the aforementioned scenarios.

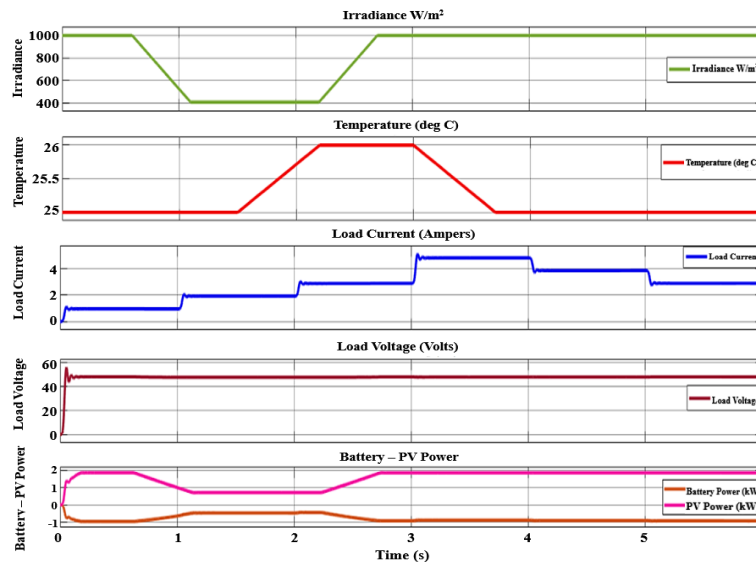


Figure 13. Results from simulations of the SPV and battery system

## 5. CONCLUSION

Operating a standalone DC microgrid poses challenges as the DC microgrid itself must ensure voltage stability. This article presents an initial investigation into developing a controller for regulating DC/DC converters and compares it with alternative control mechanisms for an independent DC microgrid. The evaluation of system performance illustrates that the bus voltage can be effectively controlled to the desired level, and the converter's potential output strength is promptly regulated when there are changes in reference or load. The research demonstrates the successful development and implementation of the proposed technique within a DC microgrid, effectively maintaining voltage stability in a standalone DC microgrid. Furthermore, the fuzzy controller employed in the DC microgrid exhibits excellent performance in various transient conditions, including rapid voltage reference tracking and accommodating load fluctuations.

## REFERENCES

- [1] Q. Yang, D. An, W. Yu, Z. Tan, and X. Yang, "Towards stochastic optimization-based electric vehicle penetration in a novel archipelago microgrid," *Sensors (Switzerland)*, vol. 16, no. 6, p. 907, Jun. 2016, doi: 10.3390/s16060907.
- [2] B. Li, S. Huang, and X. Chen, "Performance improvement for two-stage single-phase grid-connected converters using a fast DC bus control scheme and a novel synchronous frame current controller," *Energies*, vol. 10, no. 3, p. 389, Mar. 2017, doi: 10.3390/en10030389.
- [3] M. Yazdani and A. Mehrizi-Sani, "Distributed control techniques in microgrids," *IEEE Transactions on Smart Grid*, vol. 5, no. 6, pp. 2901–2909, Nov. 2014, doi: 10.1109/TSG.2014.2337838.
- [4] D. Xu, J. Liu, X. G. Yan, and W. Yan, "A novel adaptive neural network constrained control for a multi-area interconnected power system with hybrid energy storage," *IEEE Transactions on Industrial Electronics*, vol. 65, no. 8, pp. 6625–6634, Aug. 2018, doi: 10.1109/TIE.2017.2767544.
- [5] Z. Lei, F. Wang, Y. Gao, and Y. Ruan, "Research status and application analysis of bidirectional DC-DC converters in DC microgrids," *Diangong Jishu Xuebao/Transactions of China Electrotechnical Society*, vol. 31, no. 22, pp. 137–147, 2016.
- [6] R. Katuril and S. Gorantla, "Comparative analysis of controllers for a smooth switching between battery and ultracapacitor applied to E-vehicle," *European Journal of Electrical Engineering*, vol. 20, no. 1, pp. 47–75, Feb. 2018, doi: 10.3166/ejee.20.47-75.
- [7] C. Wang, Y. Liu, X. Li, L. Guo, L. Qiao, and H. Lu, "Energy management system for stand-alone diesel-wind-biomass microgrid with energy storage system," *Energy*, vol. 97, pp. 90–104, Feb. 2016, doi: 10.1016/j.energy.2015.12.099.
- [8] D. Takei, H. Fujimoto, and Y. Hori, "Load current feedforward control of boost converter for downsizing output filter capacitor," in *IECON Proceedings (Industrial Electronics Conference)*, Oct. 2014, pp. 1581–1586, doi: 10.1109/IECON.2014.7048713.

- [9] N. Hou, W. Song, and M. Wu, "A load current feedforward control scheme of dual active bridge DC/DC converters," *Zhongguo Dianji Gongcheng Xuebao/Proceedings of the Chinese Society of Electrical Engineering*, vol. 36, no. 9, pp. 2478–2485, 2016, doi: 10.13334/j.0258-8013.psee.2016.09.021.
- [10] W. Lu, N. Zhao, S. Lang, S. Liu, and L. Zhou, "Nonlinear control of a DC/DC buck converter and its ripple compensation strategy," in *Proceedings of the Chinese Society for Electrical Engineering*, 2013, pp. 35–46.
- [11] C. Chen and S. Duan, "Optimal allocation of distributed generation and energy storage system in microgrids," *IET Renewable Power Generation*, vol. 8, no. 6, pp. 581–589, 2014, doi: 10.1049/iet-rpg.2013.0193.
- [12] L. Zhi-Lin, W. Q. Tang, and X. J. Zeng, "Voltage stability control of isolated DC micro-grid based on power feed forward," *Power Electronics*, vol. 49, no. 8, pp. 32–36, 2015.
- [13] W. Song, N. Hou, and M. Wu, "Virtual direct power control scheme of dual active bridge DC-DC converters for fast dynamic response," *IEEE Transactions on Power Electronics*, vol. 33, no. 2, pp. 1750–1759, Feb. 2018, doi: 10.1109/TPEL.2017.2682982.
- [14] B. Zhao, Q. Yu, and W. Sun, "Extended-phase-shift control of isolated bidirectional DC-DC converter for power distribution in microgrid," *IEEE Transactions on Power Electronics*, vol. 27, no. 11, pp. 4667–4680, 2012, doi: 10.1109/TPEL.2011.2180928.
- [15] M. M. Rana and L. Li, "An overview of distributed microgrid state estimation and control for smart grids," *Sensors (Switzerland)*, vol. 15, no. 2, pp. 4302–4325, Feb. 2015, doi: 10.3390/s150204302.
- [16] N. Korada and M. K. Mishra, "Grid adaptive power management strategy for an integrated microgrid with hybrid energy storage," *IEEE Transactions on Industrial Electronics*, vol. 64, no. 4, pp. 2884–2892, 2017, doi: 10.1109/TIE.2016.2631443.
- [17] F. A. Inthamoussou, J. Pegueroles-Queralt, and F. D. Bianchi, "Control of a supercapacitor energy storage system for microgrid applications," *IEEE Transactions on Energy Conversion*, vol. 28, no. 3, pp. 690–697, Sep. 2013, doi: 10.1109/TEC.2013.2260752.
- [18] H. Cai, G. Hu, F. L. Lewis, and A. Davoudi, "A distributed feedforward approach to cooperative control of AC microgrids," *IEEE Transactions on Power Systems*, vol. 31, no. 5, pp. 4057–4067, Sep. 2016, doi: 10.1109/TPWRS.2015.2507199.
- [19] X. Li *et al.*, "Observer-based DC voltage droop and current feed-forward control of a DC microgrid," *IEEE Transactions on Smart Grid*, vol. 9, no. 5, pp. 5207–5216, Sep. 2018, doi: 10.1109/TSG.2017.2684178.
- [20] R. Katuri and S. Gorantla, "Math function-based controller combined with PI and PID applied to ultracapacitor based solar-powered electric vehicle," *African Journal of Science, Technology, Innovation and Development*, vol. 13, no. 4, pp. 509–526, Jun. 2021, doi: 10.1080/20421338.2020.1857542.
- [21] Y. Li, Q. Sun, D. Wang, and S. Lin, "A virtual inertia-based power feedforward control strategy for an energy router in a direct current microgrid application," *Energies*, vol. 12, no. 3, p. 517, Feb. 2019, doi: 10.3390/en12030517.
- [22] R. Katuri and S. Gorantla, "Analysis of math function based controller for a smooth transition between battery and ultracapacitor," *Mathematical Modelling of Engineering Problems*, vol. 5, no. 4, pp. 386–394, Dec. 2018, doi: 10.18280/mmep.050416.
- [23] C. Wang, X. Li, L. Guo, and Y. W. Li, "A nonlinear-disturbance-observer-based DC-Bus voltage control for a hybrid AC/DC microgrid," *IEEE Transactions on Power Electronics*, vol. 29, no. 11, pp. 6162–6177, Nov. 2014, doi: 10.1109/TPEL.2013.2297376.
- [24] L. Benadero, R. Cristiano, D. J. Pagano, and E. Ponce, "Nonlinear analysis of interconnected power converters: a case study," *IEEE Journal on Emerging and Selected Topics in Circuits and Systems*, vol. 5, no. 3, pp. 326–335, Sep. 2015, doi: 10.1109/JETCAS.2015.2462017.
- [25] G. Sun and Z. Ma, "Practical tracking control of linear motor with adaptive fractional order terminal sliding mode control," *IEEE/ASME Transactions on Mechatronics*, vol. 22, no. 6, pp. 2643–2653, Dec. 2017, doi: 10.1109/TMECH.2017.2766279.
- [26] Y. Yin *et al.*, "Observer-based adaptive sliding mode control of NPC converters: an RBF neural network approach," *IEEE Transactions on Power Electronics*, vol. 34, no. 4, pp. 3831–3841, Apr. 2019, doi: 10.1109/TPEL.2018.2853093.
- [27] Y. Gao, F. Xiao, J. Liu, and R. Wang, "Distributed Soft Fault Detection for Interval Type-2 Fuzzy-Model-Based Stochastic Systems with Wireless Sensor Networks," *IEEE Transactions on Industrial Informatics*, vol. 15, no. 1, pp. 334–347, Jan. 2019, doi: 10.1109/TII.2018.2812771.
- [28] Z. Zhu, Z. Zhao, H. Cui, and F. Shi, "Improved T-S fuzzy control for uncertain time-delay coronary artery system," *Complexity*, vol. 2019, pp. 1–11, May 2019, doi: 10.1155/2019/3864843.
- [29] A. K. Gupta and R. Saxena, "Review on widely-used MPPT techniques for PV applications," in *2016 International Conference on Innovation and Challenges in Cyber Security (ICICCS-INBUSH)*, Feb. 2016, pp. 270–273, doi: 10.1109/ICICCS.2016.7542321.

## BIOGRAPHIES OF AUTHORS



**Kalangiri Manohar**    received B.Tech. and M.Tech. degree in Electrical and Electronics Engineering from JNTU Hyderabad, JNTU Anantapuramu. His research interests are renewable energy systems, smart grid in power system, and hybrid electric vehicles. He can be contacted at email: kalangirimanoahar23@gmail.com.



**Dr. Kottala Padma**    received B.Tech. (2005) in Electrical and Electronics Engineering from Sri Venkateswara University, Tirupathi, M.E. degree (2010), and Ph.D. (2015) from Andhra University, Visakhapatnam, Andhra Pradesh. Her research interests are soft computing techniques, IoT technologies, renewable energy systems, and microgrids. She can be contacted at email: padma315@gmail.com.